JOM, Vol. 72, No. 1, 2020
https://doi.org/10.1007/s11837-019-03345-7

Synthesis of Coarse-Grained Tungsten Carbide Directly from Scheelite/Wolframite by Carbothermal Reduction and Crystallization

FENGLONG SUN,[1] XINGYU CHEN,[1] and ZHONGWEI ZHAO[1,2,3]

1.—School of Metallurgy and Environment, Central South University, Changsha 410083, People's Republic of China. 2.—Key Laboratory for Metallurgy and Material Processing of Rare Metals, Central South University, Changsha 410083, People's Republic of China. 3.—e-mail: zhaozw@csu.edu.cn

A novel method is proposed in this study to synthesize coarse-grained tungsten carbide (WC) directly from scheelite/wolframite concentrates. The synthetic process was divided into two parts, carburization and crystallization. WC was enriched in iron melt with the increase of temperature and further purified by crystallizing during the cooling process. The thermodynamics calculation for the reduction process and phase diagram analysis for crystallization were investigated. The scanning microscope (SEM) showed that the obtained sample was on the millimeter scale with a tri-prism shape, and all peaks detected by x-ray diffraction matched well with the WC structure. This method will shorten the WC preparation process greatly, and the obtained coarse-crystalline WC may have potential application in conventional cemented carbide, especially for mining and construction tools.

INTRODUCTION

Tungsten carbide (WC), the most important product of tungsten, is usually prepared with tungsten metal powders and carbon black at temperatures as high as 1400–1800°C under high vacuum or highly purified reducing gas atmosphere.[1] Meanwhile, the general process of synthesizing tungsten metal is complicated and can be described as follows. Tungsten concentrates, mainly as scheelite ($CaWO_4$) or wolframite ($Fe/MnWO_4$), are leached with alkali or acid, and the obtained tungsten solution is then purified to prepare ammonium paratungstate (APT) ($(NH_4)_{10}H_2W_{12}O_{42}$).[2] APT is heated and decomposed into tungsten oxides[3] ($WO_3/WO_{2.90}/WO_{2.72}/WO_2$), and metal tungsten is finally acquired through hydrogen reduction. The preparation process is expatiatory and costly; especially the coarse-grained WC needs more operations. Therefore, shortening the WC production process is necessary.

Various methods have been reported for the direct synthesis of WC. The US Bureau of Mines demonstrated a process in which, by mixing scheelite concentrate, sodium chloride (NaCl) and sodium metasilicate (Na_2SiO_3) together at 1050°C, halide-tungstate ($Na_2WO_4{\cdot}3NaCl$) was separated from $NaCl\text{-}Na_2SiO_3\text{-}CaWO_4$ because of the density difference, and WC was produced by methane sparging the molten halide-tungstate phase.[4] However, during the decomposition process, tungsten W existed as oxide, and many other impurities were mixed up with halide-tungstate, which could not be removed efficiently. The reduction process of molten halide-tungsten by methane was complex and its operation difficult. Kennametal Inc. developed a macro-process in which W was reduced from tungsten concentrates directly by Al and separated from the other oxides, and WC was further obtained by carburization with CaC_2 at a temperature > 2500°C.[5] This technology had a rapid reaction rate because of the high temperature but released a mass of heat and gas, making the operation more difficult, too. Moreover, scheelite and wolframite can also be reduced and carburized directly with quantities of carbon at a certain temperature.[6–10] However, many oxides ($Na_2O/K_2O/SiO_2/CaO/Al_2O_3$)were mixed up with WC and hard to remove whether by alkali or acid, even HF, because of the nanoscale of WC, which definitely influences the properties of cemented carbides made by these WC powders.

(Published online February 7, 2019)

According to the Ellingham diagram and thermodynamic calculations, wolframite could be reduced by carbon and further carburized to WC at an experimental temperature (800°C),[10] while other oxides (K_2O, MnO, SiO_2, Al_2O_3) could not be reduced, and the similar circumstance for scheelite was 1025°C.[11] However, the impurities in ores are difficult to remove, and the excess carbon restricts its actual use tremendously. On the other hand, considering the solubility of tungsten in iron, Niu et al.[12,13] investigated an iron-based composite reinforced by in situ formed WC, which grew in the iron melt from a tungsten wire, and the WC crystallized in the pig iron was pure and coarse-grained. Thus, the iron-based composite exhibited higher resistance to plastic deformation and scratch due to the WC, which crystallized in the cooling process. In view of the characteristics of the two techniques mentioned above, it was believed that qualified and ultra-coarse WC[14–16] can be prepared directly from tungsten concentrates by combining the reduction and crystallization together.

Considering the impurities and reaction-intense limits, a novel method was proposed in this study to synthesize coarse-grained WC directly from scheelite/wolframite concentrates. The carbothermal reduction and the crystallization process were systematically investigated. This method will shorten the production process of WC greatly in a smooth way and decrease the cost and amount of effluent.

EXPERIMENTAL PROCEDURE

Analytical grade reagents (≤ 74 μm) were used for all reactions. Scheelite ($CaWO_4$) was produced by Shizhuyuan, China, and the major components in mass were $CaWO_4$ (61.30%), CaF_2 (18.38%), $CaCO_3$ (15.78%), $CaMoO_4$ (1.90%), SiO_2 (1.22%), FeO (0.57%), Al_2O_3 (0.52%), MnO (0.20%) and K_2O (0.12%); wolframite (Fe/MnWO4) was procured from Jiangxi Province, China, and the components were $FeWO_4$ (51.70%), $MnWO_4$ (30.72%), SiO_2 (4.75%), CaO (2.60%), Al_2O_3 (4.18%), FeS_2 (3.59%), SnO_2 (0.39%), K_2O (0.72%), $CuFeS_2$ (0.68%), MgO (0.48%) and ZnO (0.19%). Iron and graphite powders, Al_2O_3 and SiO_2 were purchased from Sinopharm Chemical Reagent Co., Ltd. The purity of these materials was > 99.9%.

The raw material was composed of graphite, scheelite/wolframite, Fe, Al_2O_3, SiO_2 and CaO. Among these, graphite was prepared 50% more than the stoichiometry of reaction (1). Here, Ca/Fe/Mn was represented by Me. The mass ratio of tungsten and total iron, including iron from ores, was 1:1, while the ratio of Al_2O_3, SiO_2 and CaO was 4:4:2. Here, vibration milling was used to mix the powders together.

$$MeWO_4 + 5C \rightarrow Me + WC + 4CO \quad (1)$$

Mixed powders were filled into a crucible, sintered at 1150°C for 2 h in the vacuum and then further heated to 1700°C for 1 h. After complete crystallization and cooling, the bottom metal was separated and washed with acid to remove iron. The dried product was characterized to investigate the formation of tungsten carbide in the process.

To determine the phase transition, the mixed powder of scheelite/wolframite and graphite was also sintered at a temperature from 600°C to 1150°C and then analyzed by x-ray diffraction. To investigate the crystallization process, the metallic phase was cut and polished, and the cross section was detected by scanning electron microscopy (SEM).

Both the raw materials and final products were dried and then ground for further analysis. Scanning electron microscopy (SEM, JEOL JSM-6360-LV) was used to characterize the morphology. The x-ray diffraction analysis (XRD, Cu Kα, Rigaku, D/max-7500, 10°/min) was employed to analyze the crystalline structure and identify the phase. The content of Fe and W in slag was measured by inductively coupled plasma-optical emission spectroscopy (ICP-OES) (ICAP 7000) after being dissolved in solution.

Table I. Thermodynamic properties of substances related to the reduction reaction

Substance	$\Delta_f H_m^\Theta$ J mol^{-1}	S_m^Θ J mol^{-1} K^{-1}	$C_{p,m} = (a + bT + cT^{-2} + dT^2)$ J mol^{-1} K^{-1}			
			a	$b \times 10^3$	$c \times 10^{-5}$	$d \times 10^6$
CaWO4	− 164,1000	126.6	134.56	20.67	− 24.4	0
FeWO4	− 1,190,010	131.8	121.922	36.777	− 2.804	0.001
MnWO4	− 1,305,826	140.582	120.678	36.508	− 3.688	0.008
WC	− 40,166	32.384	43.376	8.636	− 9.318	− 1.021
C	0	5.74	− 0.299	11.491	0.001	83.49
MnO	− 385,221	59.71	42.133	16.956	− 2.409	− 4.206
CO	− 110,541	197.661	29.304	− 2.905	0	7.925
CaO	− 634,920	38.1	17.352	122.756	− 1.375	− 117.091
W	0	32.618	19.652	30.75	− 0.626	− 42.878
Fe	0	27.28	19.867	21.972	− 0.0994	− 3.193

RESULTS AND DISCUSSION

To investigate the possibility of the carbothermal reduction of $CaWO_4$, $FeWO_4$ and $MnWO_4$, the relationship between the Gibbs free energy and temperature was calculated. The data of standard enthalpies of formation, standard entropy and heat capacity about the substances related to the reduction are listed in Table I.[17]

The standard enthalpy (3), entropy (4) and capacity (5) of the reaction (2) were calculated as follows:

$$CaWO_4 + 3C \rightarrow CaO + W + 3CO \quad (2)$$

$$\Delta_r H_m^{\Theta}(298\ \mathrm{K}) = \Delta_f H_m^{\Theta}(\mathrm{CaO, s}) + 3\Delta_f H_m^{\Theta}(\mathrm{CO, g}) - \Delta_f H_m^{\Theta}(\mathrm{CaWO_4, s}) = 674457\ \mathrm{J\ mol^{-1}} \quad (3)$$

$$\Delta_r S_m^{\Theta}(298\ \mathrm{K}) = S_m^{\Theta}(\mathrm{CaO, s}) + S_m^{\Theta}(\mathrm{W, s}) + 3S_m^{\Theta}(\mathrm{CO, g}) - S_m^{\Theta}(\mathrm{CaWO_4, s}) - 3S_m^{\Theta}(\mathrm{C, s}) = 519.881\ \mathrm{J\ mol^{-1}\ K^{-1}} \quad (4)$$

$$\Delta_r C_{p,m} = \Delta C_{p,m}(\mathrm{CaO, s}) + \Delta C_{p,m}(\mathrm{W, s}) + 3\Delta C_{p,m}(\mathrm{CO, g}) - \Delta C_{p,m}(\mathrm{CaWO_4, s}) - 3\Delta C_{p,m}(\mathrm{C, s}) = -8.747 + \frac{89.648}{10^3}T + \frac{22.396}{10^{-5}}T^{-2} + \frac{-386.664}{10^6}T^2 \quad (5)$$

Like for $FeWO_4$, $MnWO_4$ and WC, the results are shown in Table II.

The Gibbs free energy in the reaction was calculated by the entropy and enthalpy change, which were all the function of temperature. To simplify the calculation process, $C_{p,m}$ was roughly calculated as $C_{p,m} = a + bT$.

$$\Delta_r H_m(T) = \Delta_r H_m^{\Theta}(298\ \mathrm{K}) + \int_{298}^{T} \Delta C_p \mathrm{d}T \quad (6)$$

$$\Delta_r S_m(T) = \Delta_r S_m^{\Theta}(298\ \mathrm{K}) + \int_{298}^{T} \frac{\Delta C_p}{T} \mathrm{d}T \quad (7)$$

$$\Delta_r G_m(T) = \Delta_r H_m^{\Theta}(T) - T\Delta_r S_m^{\Theta}(T) \quad (8)$$

The calculated relationship between the Gibbs free energy and temperature was plotted in Fig. 1. Thermodynamic analysis indicated that the ΔG_T of the reaction among $CaWO_4$, $FeWO_4$, $MnWO_4$ and C was negative at a temperature > 834°C, 765°C and 835°C, respectively. Furthermore, the ΔG_T of carburization between W and C was negative in all reaction temperature ranges, meaning that the reaction can take place spontaneously if tungsten is generated.[18] However, limited by solid reaction kinetics, the actual reaction temperature is higher than the theoretical value.

Figure 2a and b displays the XRD patterns of the carburized product obtained from milled scheelite and wolframite with graphite at a different temperature for 2 h. It was clear that the scheelite was reduced and carburized when the temperature was > 1100°C. Wolframite was reduced at 1000°C, followed by the generation of $(Fe/Mn)_3W_3C$, further combined with the graphite and then turned to WC with the increase of temperature. The possible reactions during these carbothermal reduction processes are listed in Eqs. 9–12. The reaction of scheelite might be divided into two steps: the generating process of tungsten from the reductive reaction (Eq. 2) and the carburization reaction of tungsten and graphite (Eq. 9).[19] The reaction of

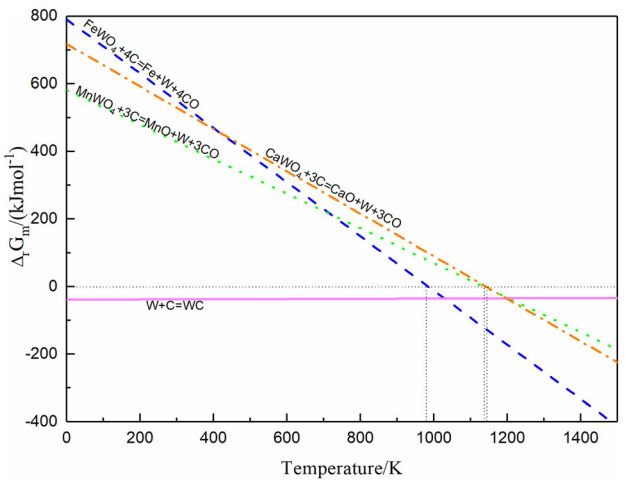

Fig. 1. Thermodynamics of reduction and carburization of scheelite and wolframite.

Table II. The thermodynamic data of the carbothermal reductions

Reactions	$\Delta_r H_m^{\Theta}$ J mol^{-1}	$\Delta_r S_m^{\Theta}$ J mol^{-1}K^{-1}	$C_{p,m} = (a + bT + cT^{-2} + dT^2)$ J mol^{-1} K^{-1}			
			a	$b \times 10^3$	$c \times 10^{-5}$	$d \times 10^6$
$CaWO_4$ + 3C = CaO + W + 3CO	674,457	519.881	− 8.747	89.648	22.496	− 386.664
$FeWO_4$ + 4C = Fe + W + 4CO	747,846	695.782	36.009	− 41.639	2.0746	− 348.332
$MnWO_4$ + 3C = MnO + W + 3CO	588,982	527.509	29.916	− 31.99	0.65	− 273.78
W + C = WC	− 40,166	− 5.974	24.023	− 33.605	− 8.693	− 41.633

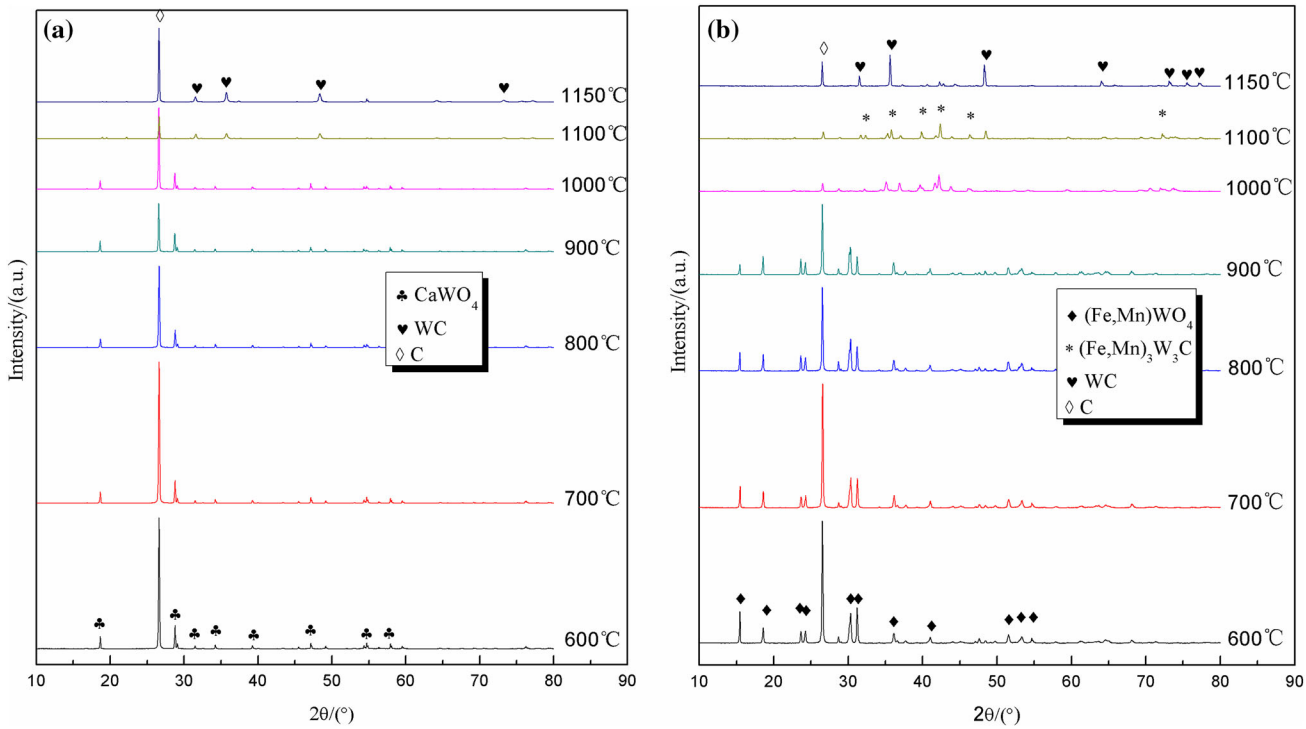

Fig. 2. XRD patterns of the carburized product obtained from milled (a) scheelite/(b) wolframite and graphite at different temperatures.

wolframite possibly consisted of three parts: reduction (Eq. 10), primary carburization to the ternary compounds W_3Fe_3C (Eq. 11)[20] and ultimate carburization (Eq. 12).

$$W + C \rightarrow WC \quad (9)$$

$$FeWO_4 + 4C \rightarrow Fe + W + 4CO \quad (10)$$

$$3Fe + 3W + C \rightarrow W_3Fe_3C \quad (11)$$

$$W_3Fe_3C + 3C \rightarrow 3WC + Fe_3C \quad (12)$$

Due to the ultra-high melting point of tungsten[21] and graphite, it was difficult to obtain coarse-grained single WC crystals from sintering. On this occasion, melt-grown, by which single crystals grew, was an effective method. In this experiment, because of the better wettability between tungsten and iron,[22] when the iron was melted, the tungsten carbide that was reduced from the ore dissolved instantaneously in the iron melt. Meanwhile, the oxide impurities were separated into the slag. The molten melt containing a high tungsten content and carbon was formed at 1700°C and converted into a supersaturated solution during cooling. Based on the composition of the melt, indicated by the red dot in Fig. 3, WC was the first component to solidify during cooling (Eq. 13), doing so congruently. Further cooling brought the liquidus to the WC/M_6C liquidus boundary, at which time joint precipitation of WC and W_3Fe_3C occurred (Eq. 14). As solidification continued, the path passed through a class II four phase equilibrium where a portion of the

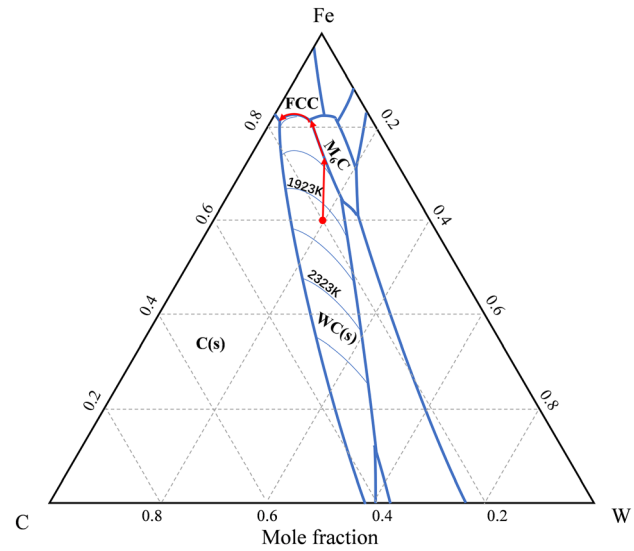

Fig. 3. Liquidus projection of the Fe-W-C ternary system.[23]

W_3Fe_3C redissolved leading to the formation of WC + γ-Fe (Eq. 15). Finally, solidification reached the ternary eutectic (Eq. 16) resulting in the formation of WC, γ-Fe and graphite.

$$L \rightarrow WC \quad (13)$$

$$L \rightarrow WC + W_3Fe_3C \quad (14)$$

$$L + W_3Fe_3C \rightarrow \gamma Fe + WC \quad (15)$$

$$L \rightarrow \text{graphite} + WC + \gamma Fe \quad (16)$$

As a result, most of the tungsten converted into WC, with a smaller fraction dissolved in the α-Fe or contained in the W_3Fe_3C phase. Figure 4 shows the polishing surface of the metallic phase. According to area statistics from Fig. 4, WC occupied 34.48% of the area, and α-Fe accounted for 52.53%; the rest was W_3Fe_3C and graphite. Considering the density of each part, the tungsten in WC took up > 80% of the total tungsten that existed in WC, W_3Fe_3C and α-Fe. The percentage of WC is influenced by the temperature, cooling rate and W/Fe/C mass fraction, which will be investigated in further experiments.

To obtain the pure and single WC crystals, a mixed acid of hydrochloric acid (HCl) and phosphoric acid (H_3PO_4) was employed to eliminate impurities. The iron was easily dissolved with hydrochloric acid, and the ternary compound W_3Fe_3C was removed by the synergistic effect of phosphoric acid in the form of a soluble acid ($H_3[P(W_3O_{10})_4]\cdot xH_2O$), which avoided the insoluble tungstic acid (H_2WO_4). The soluble phosphotungstic heteropoly acid could be recovered by a hydrometallurgy method, such as solvent extraction.[24] The SEM images of the pure and single WC crystals are displayed in Figs. 5a and b. The tri-prism shape was sized from 100 μm to 300 μm under different cooling rates and could even reach several micrometers (Fig. 5c) at a cooling rate of 1°C/min. In addition, the surface of the WC was smooth, indicating good crystallinity. Figure 5d shows the appearance of particles milled from the WC crystals and also that the positions of all the diffraction peaks match well with the WC (JCPDF 25-1047) (Fig. 6).

Based on the results above, W, Fe and Mn can be chemically reduced by graphite, while other oxides cannot at the experimental temperature. WC and Fe with higher density would sink into the molten melt physically, and the oxides CaO, SiO_2 and Al_2O_3 would reach up above the melt and integrate into slag.[25] Figure 7 explains the possible process in a schematic form. A transition layer might exist at the contact surface between the melt and slag, whereas the mass transfer process occurs because of the density. To further estimate the conversion rate of tungsten, the upper slag was cooled down to room temperature and detected by x-ray diffraction. The results (Fig. 8) show the main phases in slag were

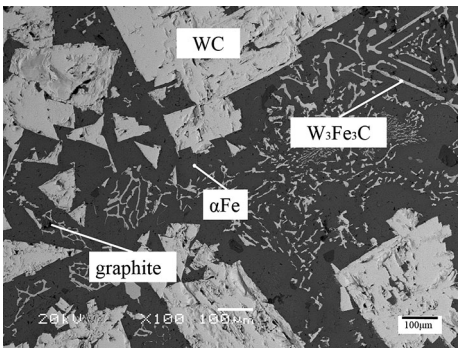

Fig. 4. Cross-section micrographs of the metallic composite at a cooling rate of − 2°C/min.

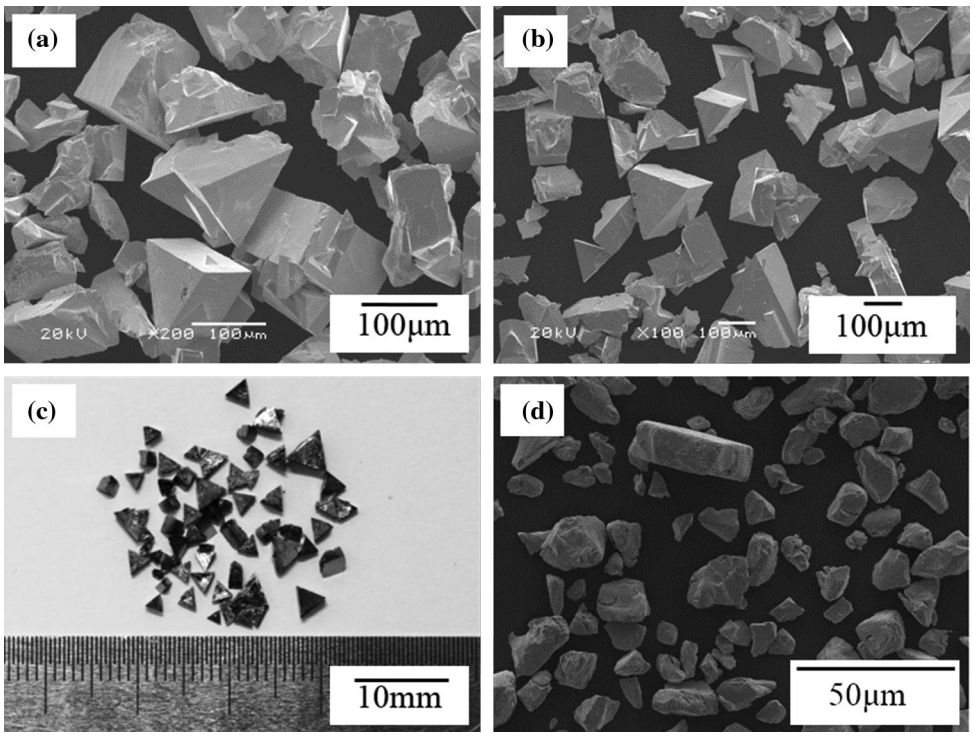

Fig. 5. Images of the specimens prepared: (a) cooling rate with − 2°C/min under ×200 magnification, (b) cooling rate with − 2°C/min under ×100 magnification, (c) − 1°C/min and (d) milled WC with the vibration mills.

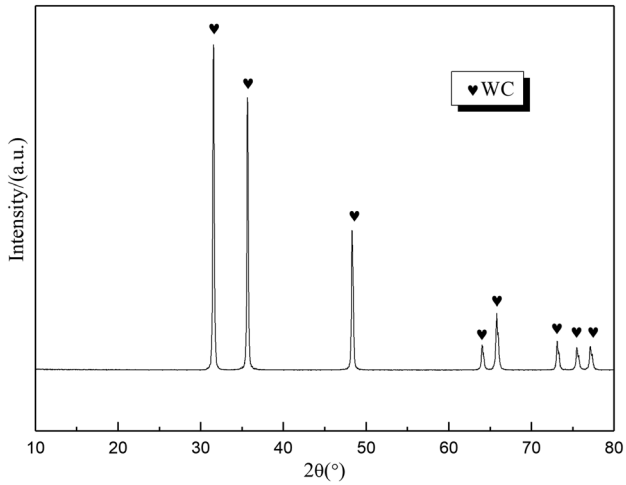

Fig. 6. XRD pattern of the milled WC powders.

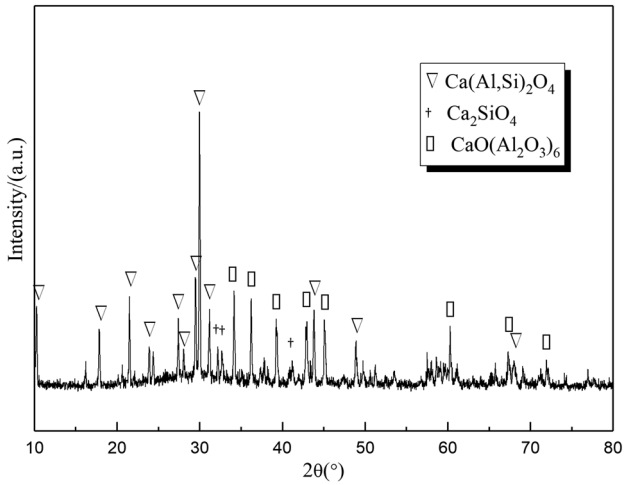

Fig. 8. XRD pattern of the slag.

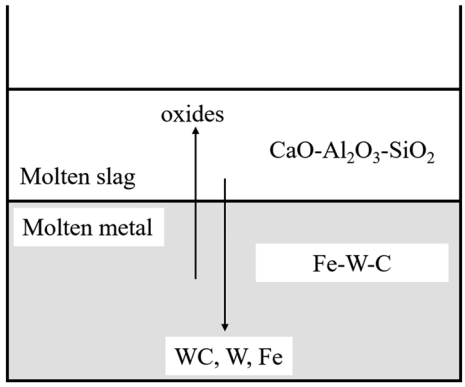

Fig. 7. Schematic diagram of separation of molten slag and melt.

yoshiokaite [$Ca(Al,Si)_2O_4$, JCPDS No. 46-1336], lamite [Ca_2SiO_4, JCPDS No. 33-0302] and hibonite [$CaO(Al_2O_3)_6$, JCPDS No. 76-0665]. Due to the complex components of the slag, it was difficult to mark all the peaks in the XRD pattern. However, the slag was proved to be the oxides of Ca, Al and Si by the experiment and analysis, which was similar to the ironmaking slag and needs to be further researched. The W content measured by ICP after dissolving the slag in solution was 0.15% in mass, meaning that almost all the tungsten sank into the melt phase in the melting process.

The above results show that in the sintering stage W was reduced and carburized to WC and in the melting stage, > 99% W was enriched into the bottom molten melt, which enabled both separation and integration of W from other oxides. Subsequently, in the cooling process, WC crystallized in the iron melt, and according to the statistics, > 80% W existed in WC. The cooled alloy was mainly composed of WC and the iron-containing phase. Meanwhile, due to the stable chemical properties of WC, which was acid-resistant and antioxidant, WC was easily separated from the iron matrix by a mixed acid of HCl and H_3PO_4. Therefore, the finally obtained WC powder was pure, and the crystal structure of the WC grain was perfect with a tri-prism shape.

CONCLUSION

Pure and coarse-grained WC crystal has been synthesized directly from scheelite/wolframite by carbothermal reduction and crystallization. The obtained WC powder was characterized by SEM and XRD, and the results showed that single WC crystals have a tri-prism shape; no other phase was found. The reduction and crystallization processes were systematically studied, which indicated that impurities in concentrates were removed into the upper slag; tungsten was gathered in the bottom metal and then gradually crystallized into WC. Compared with the conventional process, the production cycle can be greatly shortened and simplified by this method, and the operation is much easier. This study may open a new route to synthesize coarse-grained crystal transition metal carbides such as TiC/VC directly from ores or concentrates.

ACKNOWLEDGEMENTS

This work was financially supported by the National Natural Science Foundation of China (Key Program, Project 51334008) and Program for Changjiang Scholars.

REFERENCES

1. F. Medeiros, S. Oliveira, C. Souza, A. Silva, U. Gomes, and J. Souza, *Mater. Sci. Eng. A* 58–62, 315 (2001).
2. Z. Zhao, Y. Liang, and H. Li, *Int. J. Refract. Met. Hard Mater.* 289–292, 29 (2011).
3. M. Marashi, J. Khaki, and S. Zebarjad, *Int. J. Refract. Met. Hard Mater.* 177–179, 30 (2012).
4. J. Gomes, A. Raddatz, and T. Carnahan, *JOM* 29–32, 12 (1985).
5. E. Smith, *J. Cryst. Growth* 75–79, 89 (1988).
6. R. Polini, E. Palmieri, and G. Marcheselli, *Int. J. Refract. Met. Hard Mater.* 289–300, 51 (2015).

7. A. Kumar, K. Singh, and O. Pandey, *Int. J. Refract. Met. Hard Mater.* 555–558, 29 (2011).
8. N. Welham, *AIChE J.* 68–71, 46 (2000).
9. M. Sakaki, A. Behnami, and M. Bafghi, *Int. J. Refract. Met. Hard Mater.* 142–147, 44 (2014).
10. H. Singh and O. Pandey, *Ceram. Int.* 10481–10487, 41 (2015).
11. H. Singh and O. Pandey, *Ceram. Int.* 785–790, 39 (2013).
12. L. Niu, M. Hojamberdiev, and Y. Xu, *J. Mater. Process. Technol.* 1986–1990, 210 (2010).
13. L. Niu, X. Wang, and Z. Fan, *J. Wuhan Univ. Technol. Mater. Sci. Ed.* 449-454, 28 (2013).
14. J. Chi, H. Li, J. Zhao, S. Wang, M. Li, Q. Ji, and J. Li, *J. Mater. Eng. Perform.* 3859–3866, 23 (2014).
15. I. Konyashin, F. Schäfer, R. Cooper, B. Ries, J. Mayer, and T. Weirich, *Int. J. Refract. Met. Hard Mater.* 225–232, 23 (2005).
16. F. Sun, X. Chen, and Z. Zhao, *Ceram. Int.* 1434–1437, 44 (2018).
17. A. Roine, *HSC Chem.* (2006).
18. S. Bolokang, C. Banganayi, and M. Phasha, *Int. J. Refract. Met. Hard Mater.* 211–216, 28 (2010).
19. R. Yang, T. Xing, R. Xu, and M. Li, *Int. J. Refract. Met. Hard Mater.* 138–140, 29 (2011).
20. K. MacKenzie, J. Temuujin, C. McCammon, and M. Senna, *J. Eur. Ceram. Soc.* 2581–2585, 26 (2006).
21. A. Koutsospyros, W. Braida, C. Christodoulatos, D. Dermatas, and N. Strigul, *J. Hazard. Mater.* 1–19, 136 (2006).
22. C. Hanyaloglu, B. Aksakal, and J. Bolton, *Mater. Charact.* 315–322, 47 (2001).
23. K. Korniyenko, *In Iron Systems, Part 2: Selected Systems from Al-B-Fe to C-Co-Fe* (Berlin: Springer, Berlin Heidelberg, 2008), pp. 476–512.
24. Y. Liao and Z. Zhao, *JOM* 581–586, 70 (2018).
25. F. Tamura and H. Suito, *Metall. Trans. B* 121–130, 24 (1993).